SAND2010-1649P

# Solid State Lighting
# Final Topical Report

**February 15, 2010**

## Innovative Strain-Engineered InGaN Materials for High-Efficiency Deep-Green Light Emission

**Work Performed Under Agreement:**
**M6642865**

**Recipient:**
**Sandia National Laboratories[1]**
**Mail Stop 1086**
**Albuquerque, NM 87185**

**Principal Investigators:**
**Michael E. Coltrin[2] and Stephen R. Lee[3]**

**Submitted To:**

**U. S. Department of Energy**
**National Energy Technology Laboratory**
**Project Officer: Brian Dotson**
**E-Mail: Brian.Dotson@netl.doe.gov**

[1] Sandia is a multiprogram laboratory operated by Sandia Corporation, for the United States Department of Energy's National Nuclear Security Administration under contract DE-AC04-94AL8500.

[2] Phone: (505) 844-7843; Fax: (505) 844-3211; E-mail: mecoltr@sandia.gov

[3] Phone: (505) 844-7307; Fax: (505) 844-3211; E-mail: srlee@sandia.gov

## Table of Contents

## 1. Executive Summary

The goal of this project was to develop high-efficiency deep-green (≥ 545 nm) light emitters based on strain-engineered InGaN materials. Our approach to improving internal quantum efficiency (IQE) was to develop thick, strain-relaxed InGaN templates for growth of deep-green active regions. Such novel templates would enable active-region quantum wells (QWs) with lower strain than is currently possible using GaN templates. Reduced strain lowers the piezoelectric field in the QWs thereby improving light-emission efficiency. Since strain fundamentally limits indium incorporation during InGaN growth, reduced strain also raises the attainable indium composition at a given growth temperature, making longer emission wavelengths possible without suffering from enhanced defect formation at lower growth temperatures.

Over the course of this three-year project, a number of notable achievements were accomplished. Thick, strain-relaxed InGaN templates were demonstrated using AlN interlayers to induce facile strain relaxation, and thus increase indium content in the QWs. Intermittent GaN planarization layers were shown to be effective in improving roughness of the InGaN templates for indium compositions up to about 12%. We demonstrated red-shifted light emission and enhanced In-incorporation for QWs grown on strain-relaxed InGaN templates, validating the basic premise of the project. We achieved p-type doping of InGaN as high as $3 \times 10^{18}$ $cm^{-3}$. We also developed numerous processes for nanopatterning of III-N materials.

Two main obstacles limit ultimate practical implementation of this approach. First, the strain-relaxed planar InGaN templates developed under the project remain somewhat too rough and have threading dislocation densities that are much too high for subsequent growth of high-quality QWs. Second, for the nanopatterning approaches pursued in the final year of the project, the InGaN surface morphology and facet selection are difficult to control because of the lower temperatures required for InGaN-ally growth. At these reduced growth temperatures, growth surfaces invariably move towards the preferred {10-11} facet during growth. This results in pitted or serrated surface facets and prevents planar coalescence for growth of c-plane InGaN materials.

## 2. Description of Work Performed on Tasks

In this section, we review project work performed over the course of the three years of the project.

### *2 (A). Work Performed on Tasks in Budget Period 1*

**Task 1: Planar Heteroepitaxy of Strain-Relaxed $In_xGa_{1-x}N$ Templates**

Task 1 work during our first year of effort focused on the evaluation of four different propriety approaches that aimed to modify the processes by which $In_xGa_{1-x}N$/GaN heterostructures undergo strain relaxation. The ultimate goal was to produce strain-relaxed InGaN templates on GaN that have a smooth surface morphology and low threading-dislocation density for InGaN compositions in the range $x$=0.08 to 0.16.

Task 1 / Approach 1: Growth of InGaN using AlN interlayers

This approach used an AlN interlayer between the GaN and InGaN epilayers, with the intent to immediately trigger plastic deformation processes, thereby circumventing the metastable InGaN growth. Using metal-organic chemical vapor deposition (MOCVD), two different series of heterostructures were grown using this approach. The first series of samples consisted of InGaN single heterolayers with a fixed thickness, $h$=150 nm, that were grown with indium compositions ranging from $x$=0.04 to 0.40. The second series of samples consisted of InGaN single heterolayers with a fixed composition near $x$=0.05 that were grown to thicknesses ranging from $h$=80 nm up to 2300 nm. In both series, 30-nm-thick AlN interlayers were grown on the GaN-sapphire templates prior to InGaN growth. Growth rates and film thickness were determined using *in-situ* optical reflectance. Following growth, these samples were characterized by x-ray diffraction (XRD), atomic force microscopy (AFM), and transmission electron microscopy (TEM).

XRD measurements of strain showed that Approach 1 produced InGaN layers where the strain relief varied from 50-100%, indicating that Approach 1 in fact induced substantial strain relaxation, as intended. AFM studies of the surface morphology showed that the rms roughness z of these heterostructures varied widely with composition and thickness: z=1.2 nm (for $h$=150 nm, $x$=0.05), z=11.3 nm (for $h$=150 nm, $x$=0.40), and z=20 nm (for $h$=2300 nm, $x$=0.04). Only the smoothest of these templates began to be suitable for high-quality multiple quantum well (MQW) growth. In addition, XRD peakwidth measurements showed that even the low-mismatch dilute-alloy templates had relatively high threading-dislocation densities approaching ~$1x10^{10}$ $cm^{-2}$. Unlike GaN, the relaxed InGaN template peakwidths were found to decrease slowly with increasing layer thickness indicating that thick templates were not an easy route to lower threading-dislocation densities. TEM experiments confirmed the dislocated microstructure inferred from the XRD measurements. As a result of these studies, continuing experiments sought to improve both the surface morphology and the threading-dislocation density of these templates.

As the thickness of the InGaN layers increased, pits associated with dislocations (v-defects) developed on the surface, due to the low growth temperature required for the InGaN growth. Approach 2 under Task 1 of this project attempted to periodically insert thin GaN planarization layers during InGaN growth to fill-in such v-defects, producing a smoother surface morphology. Two groups of experiments were performed using this approach. The first group of experiments used coherently strained InGaN heterostructures to verify the basic concept underpinning the approach and to provide growth-calibration data needed to design strain-relaxed heterostructures incorporating this approach. The second group of experiments deployed Approach 2 in combination with Approach 1 in order to modify the surface morphology of relevant strain-relaxed InGaN templates. AFM measurements found substantial improvements in surface morphology in these heterostructures. For instance, a

310-nm-thick InGaN template with $x$=0.04 had an rms surface roughness as low as 1-2 nm by AFM.

Task 1 / Approach 3: Growth on low-threading-density GaN templates

Approach 3 used specialized GaN templates with very low threading-dislocation density with the purpose of fundamentally altering the strain-relaxation mechanisms of InGaN/GaN heterostructures. To evaluate this approach, we performed a parametric growth study where the strain-relaxation mode was evaluated as a function of InGaN composition and thickness, as well as substrate dislocation density. The study comprised three different thicknesses $h$ and compositions $x$ in combination with three different implementations of the approach, with one implementation being an unmodified control heterostructure. The result was a 3x3 matrix of $In_xGa_{1-x}N$ heterostructures with compositions ranging from $x$=0.07 to 0.15 and thicknesses ranging from $h$=160 nm to 580 nm.

Following MOCVD growth, these structures were again evaluated by XRD. For the heterostructures investigated, XRD measurements found only modest differences in the degree of strain relaxations produced when Approach 3 was implemented, with the samples employing Approach 3 exhibiting slightly more metastability against relaxation than control samples. A significant problem observed at the highest composition and thickness was the tendency for the InGaN alloy to decompose during growth, as evidenced by samples that turned metallic grey or black in color. XRD measurements showed that these samples contained metallic-indium precipitates as a result of decomposition. While these initial experiments showed less promise than Approaches 1 and 2 above, we further explored other design variations in experiments performed during Budget Period 2 before ruling out the viability of this approach.

Task 1 / Approach 4: Growth of InGaN using compositionally graded heterostructures

The intent of our Approach 4, compositional grading of the InGaN, was to provide a mechanism for reducing the threading-dislocation density that results from sought-after misfit dislocation glide. This grading approach was the final heterostructure design element considered under Task 1. This approach essentially built on development of Approaches 1-3 above, and our first results were for a heterostructure that combined Approaches 1, 2, and 4. In this experiment, we produced a 620-nm-thick $In_{0.10}Ga_{0.90}N$ template that had an rms roughness as low as 1.5 nm by AFM, which was much smoother than the 7.8 nm roughness we previously observed for 608-nm-thick $In_{0.05}Ga_{0.95}N$ that used only Approach 1.

**Task 2: Epitaxial lateral overgrowth of strain-relaxed InGaN templates**

We initially processed four wafers for ELO growth of InGaN. The wafers consisted of a sapphire substrate with a low-temperature GaN buffer layer. This was followed by blanket growth of silicon nitride, then photolithographic patterning using a special ELO mask (described below), then window openings in the silicon nitride pattern were etched down to the underlying GaN buffer layer. Because of the high processing cost of these wafers, our plan was to do initial ELO growth studies on quarter-wafer sections to make our stock of patterned templates go farther.

The ELO mask pattern used was designed to extract a great deal of information about ELO growth kinetics in a single deposition run. Absolute growth rates in ELO appear to be a very strong function of pattern dimension, i.e., the size of the window and mask regions. In previous work on GaN ELO, we found that growth from different feature sizes obeyed very simple scaling laws when the length scales were non-dimensionalized by dividing by $w$, the window opening [Ref: M. E. Coltrin and C. C. Mitchell, *J. Cryst. Growth*, **261**, 30-37, 2004]. No matter the pattern dimension ($w_i$, window opening for pattern $i$; $m_i$, mask dimension; or $P_i$, the "pitch" or $w_i+m_i$), growth of the ELO features (scaled by $w_i$) appeared to scale smoothly according to a dimensionless growth "time" $\tau$, defined as

$$\tau = \frac{GP_i t}{w_i^2},$$

where $G$ is the blanket growth rate and $t$ is the growth time. Thus, from a single growth run, examining the grown feature dimensions from the different pattern sizes is equivalent to doing a series of growths of varying growth times when analyzed in terms of the dimensionless feature size and dimensionless time $\tau$.

The ELO "Kinetics Mask" that we used contains 15 different sets of patterned line dimensions ranging from $w$=12 μm and $m$=2.5 μm to $w$=2 μm and $m$=398 μm. The range of patterns on the mask spans a factor of 1000 in the dimensionless growth time $\tau$ for the same actual growth run.

InGaN was grown on a silicon nitride masked GaN base layer in our first attempt at ELO for this task. The growth temperature for the experiment was 850 °C, and the sample was grown to a thickness of ~ 100 nm. Flow conditions for Ga and In flow were used which were expected to result in an InGaN film with an indium concentration of ~ 5 %.

Using Nomarski contrast microscopy we observed that for narrow masked regions the InGaN growth was selective on the exposed GaN windows, and the InGaN did not significantly wet the mask. However as the width of the mask region increased and the GaN window decreased, there was an increase in the amount of polycrystalline InGaN nucleation on the silicon nitride masked regions. On large masked regions the polycrystalline InGaN appeared uniform but decreased in number density in the masked region closest to the exposed GaN windows.

**Task 3: Growth of High-Indium-Composition Active Regions on Strain-Relaxed InGaN**

We conducted experiments to grow InGaN/GaN multiple-quantum-well (MQW) active regions on top of the strain-relaxed InGaN templates described above in Task 1. MQWs were grown on two strain-relaxed templates prepared using only Approach 1 and on two additional strain-relaxed templates prepared using Approach 1 in combination with Approach 2. The nominal design of the MQW active regions consisted of 2.5-nm-thick $In_{0.14}Ga_{0.86}N$ wells and 10-nm-thick GaN barriers; depending on the sample, five-, six-, or ten-period structures were grown. The thickness $h$, indium composition $x$, and rms roughness z of the four InGaN templates that were used were (1) $h$=2300 nm, $x$=0.036, $z$=20 nm; (2) $h$=370 nm, $x$=0.060, $z$=9 nm; (3) $h$=310 nm, $x$=0.037, $z$=1-2 nm; and (4) $h$=620 nm,

$x$=0.103, $z$=1.5-3 nm. For comparison purposes, similar MQWs were concurrently grown on standard GaN/sapphire templates during each growth run.

Following growth, the MQW heterostructures were characterized using XRD ω/2θ scans of the (0002) reflection. The 5-period MQWs grown on both of the rougher templates (those grown using only Approach 1) exhibited little or no superlattice satellite structure consistent with poor long-range coherence of the MQW superlattice due to the high roughness. In contrast, a six-period MQW structure grown on the smoother $x$=0.037 template (prepared using the combined Approaches 1 and 2) did exhibit clear superlattice satellites by XRD. This improved XRD result directly reflects the substantial improvement in surface morphology attained by adding Approach 2. A 10-period MQW structure grown on the smooth $x$=0.10 template did not fair as well. Here, the XRD satellite structure, though visible, was badly degraded relative to that seen for the smooth $x$=0.037 template. The higher threading-dislocation density of this template, combined with the thicker 10-period structure, led to a dense array of v-defects within the MQW region as observed by AFM and SEM. The increased roughening due to these v-defects caused the degraded XRD satellite structure.

Room-temperature photoluminescence (PL) was used to study the optical properties of the MQWs grown on the strain-relaxed InGaN, as well as the control MQWs simultaneously grown on GaN/sapphire. The four QW samples grown on relaxed InGaN templates emitted at wavelengths ranging from λ=444 nm all the way up to λ=531 nm, while the monitor QW samples grown on GaN emitted at wavelengths ranging from λ=431 nm up to λ=462 nm. The large increase in wavelength for the QWs grown on InGaN mainly resulted from the varying compositions of the InGaN templates. The smaller variation in wavelength for the corresponding GaN monitor samples resulted from intentional changes in the QW growth temperatures for some of the runs.

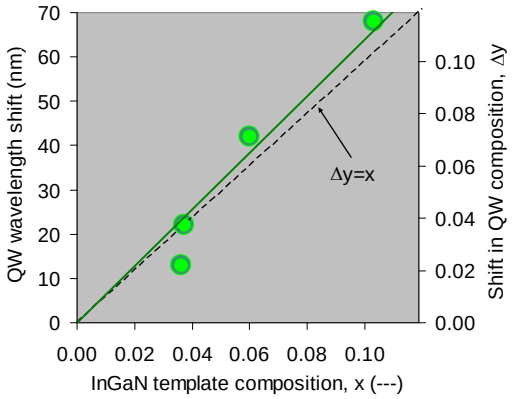


**Figure 1.** Shift of PL emission wavelength for MQWs grown on strain-relaxed $In_xGa_{1-x}N$ templates relative to MQWs simultaneously grown on GaN. The shifts in QW composition for growths on InGaN are estimated from the measured PL-wavelength shifts using the slope of the InGaN bandgap.

Figure 1 shows the shift in PL emission wavelength that occurred for the QWs grown on relaxed InGaN relative to the similar QWs concurrently grown on GaN. We consistently found a clear redshift of the PL-emission wavelength with the magnitude of the shift rising in a linear fashion with InGaN template composition.

Assuming that the QW thickness was roughly similar for the growths on both InGaN and GaN, we can roughly estimate the increase (Δy) in the composition of the InGaN QWs by dividing the wavelength shift by the local slope of the composition-dependent InGaN bandgap. These estimated shifts in composition are shown by the secondary scale on the right-hand side of the plot in Figure 1. The increase in QW composition roughly equaled the composition of the underlying strain-relaxed InGaN template, which supported our

premise that these relaxed InGaN templates would promote higher indium incorporation into the QW active region.

While these QW wavelength shifts were promising, the observed emission intensity of the QW samples on relaxed InGaN was uniformly poor irrespective of any improvements in the surface morphology for some of the templates. These poor intensity results indicate the importance of reducing the high threading-dislocation densities already noted in Task 1.

**Task 4: Growth of p-type doped InGaN films**

For the higher indium content InGaN films and quantum wells in this project, lower thermal budget p-type contact layers are needed to avoid thermal degradation of the underlying InGaN layers. We typically grow p-type AlGaN and GaN layers at 970 ºC for blue (~470 nm) wavelength LEDs and 930 ºC for green (~525 nm) wavelength LEDs. For wavelengths longer than green of interest in this project (~550 nm), even lower growth temperatures are necessary, which typically results in poor quality p-type material and reduced hole concentrations. Instead, for the current project, p-type InGaN and InAlGaN layers were developed for the p-side contact layers.

We began development of p-type InGaN films on GaN templates on sapphire. For these growths, the temperature was varied from 830 to 870 ºC to control the indium content in the films; eventually a growth temperature of 830 ºC was chosen since 4-5% indium content could be routinely achieved at this temperature. X-ray diffraction was used to determine the indium content and strain state of the InGaN films. The InGaN films were all coherently strained to the underlying GaN template. Approximately 1-μm-thick p-type GaN films were grown at a growth rate of 0.7 μm/hour, while for the p-type InGaN films, 0.2-μm-thick films were grown at a rate of 0.1 μm/hour. The thickness of the p-type InGaN films was verified using a white-light thickness mapper (RPM 2000) by subtracting the initial GaN template thickness from the InGaN-plus-GaN film total thickness.

The hole concentrations were measured by Hall Effect and the resistivities were examined for p-type GaN and InGaN as a function of the Mg precursor flow rate. A maximum in the hole concentration and a minimum in resistivity were observed for 40 sccm flow rates of the Mg precursor. For p-type InGaN; a slightly higher Mg precursor flow was needed, despite the lower growth rate. For the p-type InGaN growth, $N_2$ and $NH_3$ were the only gases used, resulting in fully activated dopants after growth and a brief anneal at 750 ºC in pure $N_2$. We determined that the hole concentration of 4-5% p-type InGaN was almost two times larger than for the p-type GaN films. We also found that the resistivity was similar for both the p-type GaN and InGaN, while the hole mobility in the InGaN was approximately one-half that in the GaN. The reason for the reduced hole mobility in the p-type InGaN may be due to the increased carrier scattering in the InGaN alloy compared to the unalloyed GaN film. From the progress gained in these initial studies we surpassed the Budget Period 1 milestone for p-type doping, and were about half way to the Budget Period 2 milestone for this Task, which was to achieve an InGaN hole concentration that exceeded $1.5 \times 10^{18}$ $cm^{-3}$.

**Work performed in support of all Tasks (MOCVD Reactor Move)**

During Budget Period 1, we were required to temporarily shut down our Veeco D-120 MOCVD reactor in order to move it from its previous location in the Compound Semiconductor Research Laboratory to the new Microsystems and Engineering Sciences Applications (MESA) facility. After moving the reactor, outside contractors affiliated with the MESA construction project installed the facilities, including gas lines, electrical, house water, and hazardous process monitoring alarms. This construction was completed in mid-March, 2007. This phase of the move required significant time for the installation itself, as well as extensive paperwork including hazardous barrier analysis, SEMI-S2 compliance, and Sandia safety levels 1 and 2 certification before reactor operation could resume. The growth chamber was rebuilt, the entire reactor and gas manifold was leak checked, and alarm shutdowns on the reactor were tested. Sandia safety level 2 was awarded and some final HPM checks were conducted, after which the ammonia, silane, and hydrogen were turned on for the first time. The source bubblers were also put on the machine.

Our Veeco D-120 MOCVD reactor was re-qualified after the move to the new MESA facility. We completed growth runs that verified the operation of the reactor, which included growth of specular GaN films on sapphire with dislocation density ~$5x10^8$ $cm^{-2}$, growth of both n-type and p-type material with electron concentrations of ~$5x10^{18}$ $cm^{-3}$ and hole concentrations of ~$5x10^{17}$ $cm^{-3}$, growth of InGaN/GaN multi-quantum well structures, and growth of light emitting diode (LED) structures. For each of the verification growth runs the original reactor-design specification were either met or exceeded. For example, some of the brightest LEDs ever produced in this Veeco D-125 reactor were produced on the first LED growth run performed after moving and recalibrating the reactor.

## *2 (B). Work Performed on Tasks in Budget Period 2*

In this section, we review project work performed during our 3-month extension to Budget Period 1 and during Budget Period 2. The Budget Period extension arose from an unavoidable delay in project work caused by the reactor move described above.

**Task 1: Planar Heteroepitaxy of Strain-Relaxed $In_xGa_{1-x}N$ Templates**

Task 1 / Approach 1: Growth of InGaN using AlN interlayers

This approach was examined during Budget Period 1; minimal further experiments were conducted during Budget Period 2.

Task 1 / Approach 2: Improvement of strain-relaxed-InGaN surface morphology using GaN planarization layers

We grew an additional series of strain-relaxed InGaN/GaN superlattices containing thin, periodic GaN layers intended to promote surface planarity in the relaxed InGaN as it grows. To promote planarization, these GaN layers must be grown at a much higher temperature than the surrounding InGaN. However, the tendency of the InGaN to decompose at higher

temperatures limits the allowable temperature for the GaN growth. We intentionally varied the growth temperature of the GaN layers in order to determine the lowest growth temperature where they remain effective.

The GaN planarization layers were quite effective at 950 ºC growth temperature and yielded an rms surface roughness as low as 0.65 nm for InGaN/GaN superlattices. As growth temperature was decreased to 920 ºC, there was an increase in roughness to 1.2 nm; further decreases in temperature produced an exponential rise in roughness. The surface was characterized by planar, overlapping platelets at 950 ºC, and as temperature was decreased, the surface developed a network of convoluted channels. At the lowest temperature examined, 906 ºC, the channeled surface converted to a denser array of fully separated mesas that gave the surface a pebble-like appearance.

The overall temperature dependence suggested that ~ 920 ºC is the lowest GaN growth temperature capable of producing a useful degree of planarization during InGaN growth. The maximum $In_xGa_{1-x}N$ composition compatible with use of GaN planarization layers grown at 920 º is limited to about x=0.12 (± 0.02); higher-composition InGaN alloys noticeably decompose during growth of GaN planarization layers.

Task 1 / Approach 3: Growth on low-threading-density GaN templates

Recall from Budget Period 1 above, the goal of this approach was to eliminate both the formation of v-defects and associated strain-relaxation modes by reducing the GaN threading dislocations that are the nucleation sites for v-defect formation. In the absence of v-defects and associated threads, previous work done at Arizona State University (ASU) [S. Srinivasan, *et al.,* Appl. Phys. Lett. **83**, 5187 (2003)] suggested that InGaN grown on GaN will shift to a more favorable strain-relaxation mode characterized by pure misfit-dislocation glide. Our work in this area during Budget Period 2 further tested this hypothesis and attempted to put it to use for producing strain-relaxed InGaN templates suitable for subsequent active-region growth.

*Optimization of Cathodoluminescence-Imaging Capabilities:*

In our Budget Period 1 experiments, it was unclear from XRD experiments whether or not the strain relaxation produced by this approach proceeded by misfit glide as suggested by Srinivasan, *et al*. Because routine imaging of the these misfits by transmission electron microscopy (TEM) is very laborious and time consuming, we decided to develop nondestructive cathodoluminescence (CL) imaging as a more efficient alternative method for detecting dislocation formation in our InGaN heterostructures.

To increase the band-edge light emission needed for successful CL imaging, we performed a detailed study of the effects of Si-doping concentration, InGaN-alloy composition, and V/III ratio on the InGaN luminescence intensity. Resulting room-temperature photoluminescence (PL) intensities (which served as a test proxy for CL-image contrast) showed a very strong dependence on Si-doping concentration for doping levels less than ~$3x10^{18}$ /$cm^3$. Above this doping level, relatively bright and constant PL intensity levels were reached, at least for $x \leq 0.15$. The overall InGaN luminescence intensity varied by a remarkable factor, up to ~1230X, for $In_xGa_{1-x}N$ compositions in the range x~0.07 to 0.18 and for Si-doping

concentrations ranging from ~$1x10^{17}$ up to ~$1.5x10^{19}$ $cm^{-3}$. These wide variations demonstrated the need for proper optimization of doping levels and growth conditions in order to obtain high-contrast CL images. Based on these results, subsequent growths of thick InGaN were Si doped at $3x10^{18}$ /$cm^3$ in order to facilitate post-growth CL imaging of dislocations.

*Inducing Long-Range Misfit-Dislocation Glide:*

In an attempt to induce long-range misfit-dislocation glide, we grew several different additional sets of thick InGaN samples on low-threading-density GaN templates. Three types of low-threading-density GaN templates were used in these studies: (i) ELO-type, (ii) ULD-type (basically, ELO accomplished using a $SiN_x$ "auto-masking" technique), and (iii) bulk GaN grown by HVPE. The threading densities for these templates ranged from ~$5x10^6$ to ~$1x10^8$ $cm^{-2}$, which was significantly less than that for our standard GaN templates on sapphire, ~$5x10^8$ $cm^{-2}$. All experiments were conducted using simultaneously grown 3-wafer sets enabled by the multi-wafer capability of our MOCVD reactor. Each set of wafers made use of two of the three types of specialty-GaN templates described above; the third wafer was always a standard GaN-on-sapphire template, which was included for comparison purposes. The influence of a variety of parameters on misfit-dislocation formation was examined in these studies; these parameters included: (i) $In_xGa_{1-x}N$ composition, which varied from x~0.09 up to x~0.17, (ii) InGaN heterolayer thickness, h, which varied from h~150 nm up to h~600 nm, and (iii) V/III ratio, which was controlled by varying the ammonia flow rate from ~5 slm up to ~15 slm. Following growth, the samples were examined by SEM/CL to image misfit dislocations, by standard SEM and/or AFM to determine surface morphology, and by XRD to determine composition and strain.

For the InGaN/GaN heterostructures and growth conditions examined, long-range misfit-dislocation glide at the InGaN/GaN heterointerface was only sporadically observed. Averaging over all experiments, only about one of every four samples showed evidence of long-range misfit-dislocation glide in CL, SEM, or AFM images. In the limited instances where long-range glide was successfully observed, the glide never produced a degree of strain relaxation greater than ~ 15%. Moreover, the occurrence of long-range glide did not appear to depend on the initial threading-dislocation density or the type of GaN template. In fact, all of the different types of GaN templates that we tried, including our standard GaN templates on sapphire, randomly showed long-range misfit-dislocation glide. Our observations failed to confirm the original hypothesis of the ASU group that the initial threading-dislocation density of the GaN fully controls the relaxation mode. The sporadic results obtained for our larger set of observations instead suggested that an uncontrolled extraneous source may control heterogeneous nucleation of the linear misfit dislocations (for example, stress-concentrating particulates introduced during sample handling, loading, or growth). At present, we are left without a means to control the poorly understood nucleation of these linear misfit dislocations.

*Alternative Modes of Strain-Relaxation in InGaN/GaN:*

Since the sought-after linear misfit dislocations either failed to appear, or failed to produce a high degree of strain relaxation even if they did appear, the dominant mode of strain relaxation always shifted to other less-desirable mechanisms as the InGaN layer

composition and thickness were increased. Broadly speaking, three different relaxation pathways were observed to compete in these heterostructures, and the resulting dominant relaxation behavior depended on the specific InGaN growth conditions.

The first pathway proceeded by "patchy" desorption of portions of the initial InGaN layer during growth, which led to an initially planar InGaN layer containing a large number of perforations or holes. InGaN tended to regrow with a rough morphology in these holes, and as the process proceeded with increasing film thickness, the surface appeared to become entirely converted to roughened InGaN through regrowth in the ever-expanding perforations.

The second pathway centered on v-defects formed at pre-existing threading dislocations or formed above the path of any linear misfit dislocations that sporadically appear in the layers. As the film thickens, stress concentrations at the base of the v-defects punch out localized dislocation loops that expand along the basal plane to surround the base of each v-defect. These floret-shaped dislocation arrays nucleate further v-defects at the periphery of each initial v-defect; the localized strain relaxation produced by these dislocation arrays simultaneously accelerates the InGaN growth rate in the same region. Both effects combine to increasingly roughening and to relax the heterolayer with increasing thickness.

The third pathway is stress-induced morphological instability of planar InGaN, which takes hold in planar regions of the InGaN layer when the first two mechanisms are less dominant. On a planar growth surface, small, random deviations from planarity tend to occur. If the heterolayer is lattice mismatched, this leads to a well-known stress-induced instability where high spots in layer grow at a different rate from low spots in the layer because of the slight differences in strain energy at each position [Asaro and Tiller, Met. Trans. **3**, 1789 (1972)]. This growth-rate instability becomes exponentially amplified with thickness, such that dense arrays of grooves eventually form all across the layer as thickness increases. In compressively strained heterolayers such as InGaN on GaN, stress concentrations at the base of these grooves concomitantly nucleate localized misfit dislocations, in manner similar to that described above for v-defects.

Unfortunately, none of these three observed pathways led to strain-relaxed InGaN with a surface morphology and threading-dislocation density suitable for growing high-IQE InGaN quantum wells. Thus, our experiments suggested that Approach 3 under Task 1 was not a suitable method for growth useful strain-relaxed InGaN templates.

Task 1 / Approach 4: Growth of InGaN using compositionally graded heterostructures

This approach was examined during Budget Period 1; minimal further experiments were conducted during the present reporting period.

Task 1 / Approach 5: Growth of InGaN using Sc interlayers

Based on our continuing need to develop an approach to lower threading-dislocation density in our relaxed InGaN successfully grown using AlN interlayers (Task 1 / Approach 1), we investigated a new interlayer growth method that involves the insertion of ScN interlayers into the heterostructure to reduce threading dislocations. While this approach was not

explicitly included in our original plan, it represented an extension of our previous Task 1 plans involving AlN and GaN interlayers. ScN interlayers has previously proved very successful for reducing threading dislocations in GaN [M. A. Moram *et al.*, Appl. Phys. Lett. **91**, 152101 (2007)], and we therefore decided to test the applicability of this scheme for our relaxed InGaN layers grown on AlN interlayers.

Scandium metal films were deposited by pulsed-laser deposition on ~3-μm-thick template layers of GaN on sapphire. These Sc films were nitrided in a MOCVD reactor by annealing under $NH_3$ flow. The effect of pressure, temperature, and time on nitrided-film uniformity was studied. It was found that the film changes from opaque-grey to transparent-yellow color when Sc converts to ScN. Energy-dispersive x-ray (EDS) spectroscopy confirmed that there was no loss of Sc during nitridation. Lower pressures and temperatures were found to yield better film uniformity.

We attempted regrowth of GaN on thick (h > 16 nm) ScN films, using a two-step process: (i) the GaN film was nucleated at reduced temperature (~800-950 $^{o}$C, depending on the sample), followed by (ii) 60 minutes of high-temperature (1050 $^{o}$C) growth. We observed poorly aligned and separated grains at the center of the wafer, well-aligned grains near the edge, and some regions of coalescence. Uniform coalescence was found to be difficult in our numerous attempts. We also attempted regrowth of GaN on ScN interlayers deposited on thick AlN templates on sapphire. Poorly aligned grains were again observed near the wafer center along with channel-fracture patterns at the wafer edge. GaN nucleation in these AlN crack arrays at the wafer edge led to ELO-like lateral GaN growth, revealing that ScN interlayers basically function as randomly self-patterned "auto-masks" for ELO, much like other thin interlayers reported in the literature ($SiN_x$, TiN).

We also attempted similar GaN regrowths on thin (h < 6 nm) interlayers. The microstructure of the regrown GaN was more uniform across the wafer surface. The films were fully coalesced, but still not adequately planar.

Reproducing the previously published ScN interlayer results for reducing dislocations in GaN proved to be more difficult than anticipated. As a result, attempts to grow InGaN films on the ScN layers were not attempted.

The work reported in this section was conducted jointly with another of our EERE funded projects "Novel ScGaN and YGaN Alloys for High Efficiency Light Emitters" (M6642867), Dan Koleske, PI. Further details are given in the final report for that project.

Task 1 / Approach 6: Growth of InGaN on thick AlN templates

Our previous work on Task 1 / Approach 1 showed that thin AlN interlayers efficiently induce strain relaxation, but at the same time, they produce high threading-dislocation densities. One thought was that the rough, three-dimensional morphology of the AlN interlayer plays a key role in generating these threads, but this rough starting surface may not in fact be needed to induce relaxation -- the relaxation may instead result primarily from growth on the more highly lattice-mismatched AlN surface. If this is true, growth on thick, planar AlN templates (instead of on rough AlN interlayers on GaN) could yield a relaxed InGaN layer with a lower threading-dislocation density. To test this idea, we grew strain-

relaxed InGaN on thick AlN templates as an extension of our original AlN-interlayer approach.

We grew 2-μm-thick AlN layers on SiC substrates and diced these wafers into quarter-wafer pieces, upon which we grew two different strain-relaxed InGaN/GaN heterostructures. Both structures consisted of a 10-period InGaN/GaN superlattice with a period of 38 nm and an InGaN/GaN thickness ratio of ~10:1 (x=0.057 for the first sample and x=0.110 for the second sample).

X-ray diffraction (XRD) was used to characterize the two strain-relaxed InGaN/GaN heterostructures grown on AlN/SiC. XRD found the expected InGaN compositions (x=0.057 and x=0.115) and a degree of strain relaxation in the 65-100% range, which was similar to the degree of relaxation we previously observed for growth on AlN interlayers. InGaN peakwidths were also similar to or exceeded those of similar structures grown on GaN using AlN interlayers. These similarly broad peakwidths suggested that InGaN growth on thick, planar AlN would not provide a viable route to reduced threading-dislocation density.

**Task 2: Epitaxial lateral overgrowth of strain-relaxed InGaN**

Task 2 / Approach 1: Micron-scale patterning

We began our studies on the FACELO approach by growing ELO GaN pyramidal stripes at 950 ºC. The pyramidal bases were 3.8 micron wide, with the base of adjacent stripes separated by just 0.2 microns. We then grew a 30-nm-thick AlN interlayer on the stripes, followed by 360-nm-thick InGaN of composition x=0.05. The purpose was to examine the strain relaxation, defectivity, and surface morphology produced when we perform InGaN FACELO on the {11-22} facets of GaN.

During post-growth characterization, the overgrown InGaN composition was found to be x=0.046, and the wafer had a smooth and specular appearance and no evidence of grey discoloration. The InGaN strain-relaxation was 59%, similar to that found for InGaN growth on unpatterned GaN templates on sapphire. We also found a reduction in the XRD symmetric (0002) peakwidth suggesting a modest decrease in threading density compared to planar growth; the extent of the reduction was not well quantified due to uncertain interpretation of peakwidths for InGaN growths conducted on the faceted stripes.

To explore facet evolution with film increasing thickness, we performed an additional regrowth on this FACELO sample (the “first regrowth”). The next regrown layer was a 5-period, 500-nm thick, x=0.075 superlattice (the “second regrowth”). The GaN portion of the superlattice was grown at 985 ºC; InGaN portions were grown at 838 ºC to maintain average superlattice composition near x=0.05. For both regrowths, SEM analysis showed formation of a basal plane at the top of the pyramidal facets, but not at the bottom of the trough. For the second regrowth, XRD analysis of the In composition suggested that In did not appreciably incorporate on the sloped {11-22} facets during the regrowth. Instead, lateral growth of the facets mainly occurred due to GaN deposition only.

A separate FACELO experiment was done in which the entire structure was grown in a single run without interrupts for inspection. An $In_{0.05}Ga_{0.95}N$ single-heterolayer was grown as a continuous alloy to a total thickness of 860 nm -- without using the InGaN/GaN superlattice approach deployed for the uppermost part of the previous sample. The goal was to compare the two samples and determine how surface-facet formation and indium incorporation are influenced by continuous growth versus superlattice growth. We observed little development of a c-plane facet at the top of the GaN pyramids, and infer that the continuously grown InGaN is conformal to the underlying pyramidal GaN stripes.

There is an anisotropic in-plane strain distribution that arises because the pyramidal stripes produce different InGaN strain-relaxation along directions parallel and perpendicular to the stripe. The inclined facet modifies the elasticity theory needed for a rigorously correct interpretation of the x-ray data. The asymmetric (20-25) reflection was used to examine in-plane strain parallel to the stripe and the asymmetric (11-24) reflection was used for strain perpendicular to the stripe. We found very different strains and compositions parallel and perpendicular to the stripe confirming the hypothesized anisotropic in-plane strain. The InGaN strain parallel to the stripe is mostly unrelaxed while strain perpendicular to the stripe is substantially relaxed.

In further XRD studies of this second sample, the InGaN regrown on the basal plane located at the apex of the GaN pyramidal stripes was found to be untilted in orientation, with an approximate composition x~0.050 and a strain relaxation near 65%. In contrast, InGaN regrown on the center of the {11-22} sidewall facets exhibited a tilted InGaN orientation, with an approximate composition x~0.024 and a strain relaxation near 50%. The facet composition was reduced by a factor of two relative to the basal plane, in agreement with trends previously observed by others where indium incorporation is reduced for higher composition quantum wells also simultaneously grown on {11-22} and {0001} facets [see, for example, Nishizuka *et al.*, APL **85**, 3122 (2004)]. A subsequent SEM/EDS analysis gave an In fraction x~0.050 at the tops of the stripes and x~0.030 on the sidewall facets, in good agreement with our XRD analysis.

A similar SEM/EDS analysis of the first FACELO sample (in which the superlattice structure described before was grown) showed the clear presence of aluminum at the top centerline region of the stripe. The fact that the AlN interlayer remains observable by EDS after subsequent InGaN and GaN regrowths supports the notion that minimal basal plane deposition occurred during these regrowths – material was instead predominately incorporated on the {11-22} facets to produce mainly lateral extension of the basal plane facet.

Due to the tendency for strongly reduced In-composition on the inclined facet and the observed conformal growth for the InGaN (which limits the prospects for planarization at the few-micron length scale), the FACELO approach to achieving strain-relaxed InGaN templates did not appear promising. Thus, our emphasis in Task 2 turned to a nanopatterning approach, described next.

<u>Task 2 / Approach 2: Nano-scale patterning</u>

Prof. Steve Brueck at the University of New Mexico (UNM) maintains an interferometric lithography (IL) laboratory capable of producing 1D stripe arrays or 2D dot arrays with critical dimensions of ~200 nm or less. To gain quick and less costly access to a large-area nanopatterning capability, we initiated a contract to UNM to obtain user access to their facility to use their IL laboratory to apply, expose, and develop nanopatterns in photoresist films, as needed to produce nanopatterned GaN to be used for subsequent regrowths of patterned, strain-relaxed InGaN. Most other supporting processes including dielectric thin-film deposition, metal thin-film deposition, metal liftoff, plasma etching, and wet etching were carried out at Sandia's MESA MicroFab cleanroom facility. This mix of processing venues allowed us to take advantage of both UNM's unique IL nanopatterning laboratory and Sandia's superior processing facilities for compound semiconductors. In particular, we minimized process-development efforts by leveraging the technical expertise, the standard processes, and the better process stability available in the Sandia MicroFab.

For the nanopatterning experiments described below we used 2-μm-thick GaN templates grown on sapphire. A plasma-enhanced chemical-vapor-deposition (PECVD) tool located within the MicroFab was used to subsequently deposit a 50-nm-thick $SiO_2$ layer. Lithography was performed using a 355-nm-wavelenth frequency tripled Nd:YAG laser. Prior to laser-interferometric exposure, a 120-nm-thick antireflective coating (Brewer Science i-CON-16) and a 500-nm-thick positive PR film (Shipley SPR505-A) were spin-deposited on the wafers and soft baked.

Once exposed by IL and developed, these samples were used to develop multi-step reactive-ion-etching (RIE) procedures for transferring the PR nanopattern onto the underlying ARC, $SiO_2$, and GaN layers. Our initial process-development efforts successfully yielded GaN nanostripes with a 500-nm pitch, a GaN stripe width of 220 nm, and a trench depth up to 250 nm. However, one challenge was the slope of the stripe sidewalls away from vertical, which produced narrowing of the trenches with increasing depth. We found that further optimization of the ICP process, conducted using 50 W of plasma rf-power and an altered sample bias, yielded nearly vertical sidewalls in the upper half of the channel, but the bottom of the channel still tapered to an undesirable point.

To remove the remaining sidewall taper, we performed experiments using a facet-selective wet-etching process recently developed in a separate program. This facet-selective etch has a very slow etch rate for {10-10} surfaces and a fast etch rate for most other surface orientations. This anisotropy allowed rapid removal of sloping sidewall materials resulting in vertical {10-10} sidewall surfaces. Since the sidewall planes here were actually along {11-20}, the sidewalls ended-up consisting of microfacets paralleling {10-10} such that the sidewall surface became microfaceted due to the selective wet etch. Nonetheless, the selective etch progressively reshaped and improved the bottom half of the channel, eventually producing straight and vertical sidewalls and a relatively flat-bottomed channel. At room temperature this process took ~110 minutes; heating the etchant to 50 °C reduced the required time to ~30 minutes.

These combined improvements to the ICP and wet etching yield more ideally shaped, high-aspect ratio GaN nanostripes that were well suited to our InGaN growth studies.

We began our study of MOCVD regrowth of InGaN on top of our initial, less-optimized, GaN nanostripe arrays (from the RIE work, described above). Our first regrowth of $In_{0.1}Ga_{0.9}N$ to a nominal thickness of 150 nm on a GaN nanostripe array produced InGaN stripes with a trapezoidal cross-sectional shape, as expected for the low growth temperature (~810 ºC) required to incorporate indium at x=0.10. Surprisingly little InGaN appeared to grow on the nanostripe sidewalls or at the bottom of the trenches formed by the sidewalls. Some limited lateral growth of the InGaN occurred at the top of the GaN stripes, and the resulting InGaN-stripe thickness and width was just short of the initial coalescence point for adjacent stripes.

A preliminary analysis of x-ray diffraction data for this InGaN/GaN nanostripe array indicated that the InGaN stripes had a composition near to the expected value of x=0.10 obtained from separate calibrations. Moreover, the InGaN stripes appeared to be unrelaxed parallel to the stripe direction and partially relaxed perpendicular to the stripe direction, just as we expected for elastic deformation of the InGaN/GaN couple due to the high-aspect-ratio geometry of the nanostripe. Fully quantitative results for the XRD analysis of composition and strain required the development of elasticity theory that takes into account the non-biaxial strains produced in the InGaN by the anisotropic stripe geometry. Further efforts to grow and achieve coalescence of nanopatterned-InGaN were carried out during Budget Period 3 as reported below.

**Task 3: Growth of high-indium-composition active regions on strain-relaxed InGaN**

In Budget Period 2 we continued efforts to grow and characterize InGaN/GaN multiple quantum well (MQW) active regions on top of strain-relaxed InGaN templates (x=0.037 and x=0.103 strain-relaxed InGaN/GaN superlattice templates). For this work, we reduced the number of MQW layers to 4 (from the previously used 10) in an effort to eliminate the extreme v-defect formation seen earlier. We also somewhat altered the InGaN regrowth buffer layer immediately below the MQWs, using a 100-nm, x=0.02 layer, and increasing the buffer growth temperature to 880 ºC to avoid v-defect formation. The rms surface roughness of the MQWs was in the 3-to-5 nm range, much better than the 14 nm seen for the 10-MQW samples. However, improved roughness approaching the 1-nm range is ultimately needed.

For these MQW samples on strain-relaxed InGaN templates, redshifts of 17-39 nm were observed, perhaps due to the lower baseline composition in the QW. The general trend reconfirms the trend previously found in Budget Period 1: the nominal increase in the QW composition produced by use of a strain-relaxed InGaN template roughly equals the In-composition of the underlying strain-relaxed InGaN template.

**Task 4: Development of p-type materials, heterostructures and thermal-activation processes**

Our work on Task 4 focused on improving the hole concentration in p-type InGaN films. These experiments involved 14 separate MOCVD growth runs composing a parametric study that investigated the influence of variations in both the $NH_3$ flow rate and the Mg-precursor flow rate. After each growth run, the hole concentration was determined using Hall-effect measurements conducted at 5 different positions on each wafer. Optical-

reflectance measurements made both before and after InGaN growth were used to accurately determine InGaN film thicknesses needed for accurate determination of hole concentrations by Hall effect. X-ray diffraction was used to measure the indium concentration and verify the InGaN strain state.

For these optimization studies, the InGaN growth rate was ~200 nm/hour and the InGaN growth temperature was 820 °C. In studies varying the $NH_3$ flow rate from 7 to 15 slm, an $NH_3$ flow rate of 15 slm combined with an $N_2$ flow 10 slm was found to produce the best incorporation of indium into the InGaN. XRD measurements found that the resulting indium concentrations ranged from 7 to 8%, and the InGaN was found to be coherently strained to the underlying GaN, as intended. The optimized $NH_3$ and $N_2$ flow conditions differ from those used in our earlier p-doping work, as lower $NH_3$ flows were used.

Following optimization of the $NH_3$ flow rate, the flow rate of the Mg precursor (bis-cyclopentadienylmagnesium or $cp_2Mg$) was coarsely varied from 40 to 120 sccm, with the highest hole concentration occurring near 80 sccm. We conducted more detailed experiments examining the effect of varying the Mg-precursor flow rate in a narrower range around 80 sccm. The average measured hole concentration and mobility were examined as a function of the Mg-precursor flow rate. The data confirmed 80 sccm as the optimum Mg-precursor flow rate, and at this flow rate, the average hole concentration maximized at ~$3.0 \times 10^{18}$ $cm^{-3}$, with individual hole concentrations ranging from $2.1 \times 10^{18}$ $cm^{-3}$ to $4.4 \times 10^{18}$ $cm^{-3}$ at various positions on the wafer. These average and maximum hole concentrations meet or exceed all p-type doping levels targeted in our milestones for Budget Period 2, and also far exceed our initial results reported in Budget Period 1. The improved results here may be due to both the differently optimized InGaN growth conditions being used and the use of InGaN with higher indium composition.

## *2 (C). Work Performed on Tasks in Budget Period 3*

### Task 2: Epitaxial lateral overgrowth of strain-relaxed InGaN

Task 2 / Approach 2: Nano-scale patterning

*Growth on nanostripes*

Further InGaN growth studies on nanostripes were explored in Budget Period 3. InGaN (x~0.10) was found to grow with a trapezoidal cross-section profile, with little growth on the nanostripe sidewalls or channel bottom. The InGaN stripes appeared unrelaxed parallel to the stripe and partially strain relaxed in the perpendicular direction.

SEM images of InGaN regrowths on GaN nanostripes for thickness of 150, 250, 350 nm showed that the InGaN grows with steeply faceted (11-22) sidewalls, the angles of which increase with thickness. Coalescence of the features was just beginning for the 350 nm regrowths. The basal plane at the top of the facet narrowed with increasing growth time and was nearly extinguished for the 350 nm growth. However, this top growth plane was very rough and pitted with v-defects.

For a subsequent 700 nm of regrowth run, initial coalescence of the nanostripe features occurred, but the periodic and faceted shape of the InGaN growth front remained constant during continued growth, with further growth producing a continuous, planar underlying layer of InGaN (whose thickness increases with time) beneath the faceted growth front. An oblique view of these facets showed that they are not smooth inclined surfaces; instead, they consisted of an array of nm-scale serrations that oscillate about the nominal {11-22} plane of the facet. We hypothesize that the serrated surfaces form because {10-11} facets are actually thermodynamically preferred, but the original larger-scale nanostripe pattern enforces the persistence of {11-22}.

As part of Budget Period 3 work, we completed developed an *XRD characterization* theory to analyze biaxial strain on the regrown InGaN. We found *unequal* in-plane strains, $\varepsilon_1$ and $\varepsilon_2$, which confirms the expected strain anisotropy for heterostructures grown in a striped geometry with strained-layer thickness comparable to the stripe width. The strain along the stripe, $\varepsilon_1$=-0.0105, was equal to or slightly less than the expected pseudomorphic strain, $\varepsilon_0$=-0.0133, indicating that the InGaN strain relaxation is small in that direction. In the direction orthogonal to the stripe, instead of being near the pseudomorphic strain, the strain perpendicular to the stripe, $\varepsilon_2$=+0.0059, rose towards zero, which would be the point of full strain relaxation, and then actually overshot to a positive value such that the films ended up in tension along this direction. This overshoot is partially driven by the noted lack of relaxation parallel to the stripes, which acts in concert with the large height-to-width aspect ratio of the regrown InGaN to produce a large *elastic* strain-relaxation response in the transverse direction. Importantly, the XRD data showed that nanopatterned growths of InGaN, where the InGaN thickness and width are comparable in size, indeed produced strong elastic relaxation of the InGaN's lattice-mismatch strain.

For the 700 nm regrowth, the composition fell from x=0.10-0.12 in the previous uncoalesced films to x=0.02-0.05 in this coalesced film. The strains along the nanostripes, $\varepsilon_1$, remained mostly unrelaxed for all films, and the less negative strain values for the coalesced layers simply reflected the reduced indium composition. For the strain perpendicular to the stripes, $\varepsilon_2$,the change was more interesting as the highly tensile strains (positive $\varepsilon_2$ values) for uncoalesced films turned compressive (negative $\varepsilon_2$ values) once adjacent stripes impinged upon each other. Coalescence reduced the ability of the stripes to lower strain energy by elastically expanding laterally and this manifested as the reversal of the strain perpendicular to the stripes.

In Budget Period 3, IL patterning work at the UNM CHTM user facility continued in order to produce 1-D stripe arrays with a reduced pitch of 350 nm (vs 500 nm previously). In addition to the narrower pitch, the mask material was switched to $SiN_x$ (from the previous $SiO_2$) with the expectation of better selectivity with the nitride mask. Much time was spent optimizing the processing steps to successfully produce these patterns. Difficulties included photoresist stripe fabrication, large defects (~100 nm) that arose during Ni-mask deposition, persistence of etching residue, optimization of the $SiN_x$ etching process, and undesired desorption, roughening, and loss of the GaN material that arises during the new processing procedures.

We conducted three growth runs aimed at producing thick strained-relaxed InGaN on these nanopatterned GaN stripes.

In the first growth, we made use of a ~30 nm AlN underlayer with the purpose of inducing rapid strain-relaxation of the InGaN layer. The AlN grew at the bottom of the trenches on GaN as intended, but then the InGaN failed to nucleate on top of the AlN and instead preferred to grow in a low-strain mode by nucleating on top of the adjacent $SiN_x$ mask, where no InGaN growth was intended. To our surprise, it appears that the AlN is even more selective against InGaN nucleation than is the amorphous $SiN_x$ mask.

We elected to repeat this same growth procedure but now without the AlN interlayer and found that all of the InGaN nucleated on GaN at the trench bottoms, and there was little or no nucleation on the $SiN_x$ mask. Thus, it appears that *both* AlN and $SiN_x$ exhibit good selectivity against InGaN growth, but the selectivity of AlN is *higher*, which gave rise to the odd result seen for the first growth. The selectivity was not quite perfect as we saw formation of a few isolated InGaN grains or crystallites located at the edges of the InGaN stripes at positions just over the $SiN_x$ mask. Nonetheless, the majority of each InGaN stripe was judged to be a single-crystal layer that was epitaxial to the underlying GaN, though most likely, partially strain relaxed.

In the last growth in this series, we doubled the InGaN layer thickness, again without the AlN interlayer, to determine how the faceting of the InGaN stripes evolves with thickness, and to see how the selectivity of $SiN_x$ holds up with thickness. The $SiN_x$ mask remained selective as lateral InGaN growth increasingly covered the mask stripes. Nominally {11-22} sidewall facets formed on the InGaN stripes due to the lateral growth, but these facets exhibited a nonplanar, serrated surface morphology. Presumably, the serrations resulted from an attempt to form preferred {10-11} oriented facets by microfaceting of the local surface. Extreme roughness persisted on the top-most basal-plane surface at the increased thickness, again consistent with trends we previously observed for unpatterned growths of InGaN. While the observed selectivity of the $SiN_x$ is promising, the persistent roughness was not compatible with subsequent quantum-well and LED growth.

A set of growth experiments were also performed to *see if lateral to vertical growth-rate ratio could be tuned through heavy Mg doping*. Unfortunately, it was found that no Indium incorporates into the heavily Mg-doped InGaN regrown on GaN nanostripe arrays. (For comparison, In did incorporate on planar growth regions during this Mg-doping experiment.) In addition, there was no significant lateral growth enhancement of the nanostripes. So, it appeared that heavy Mg-doping does not offer an attractive means for enhancing lateral growth and coalescence of the nanostripe arrays.

Recent work [Senda *et al.*, Jpn. J. Appl. Phys. **46**, L948 (2007)] suggests that the facet formation, the coalescence, and the resultant surface morphology of patterned InGaN growths vary strongly with the crystallographic orientation of the patterned GaN surface. Moreover, reduced surface roughness arises for the non-polar m-plane orientation and for certain semi-polar orientations. Consequently, any future efforts to pursue nanopatterned InGaN should strongly consider studies of these alternative crystallographic orientations -- instead of patterning the more traditional basal plane, as was done in the present work. A

practical challenge for such studies is obtaining or developing the needed non-polar GaN materials, which remain rare, expensive, and difficult to obtain in sufficient quantities.

The reduced InGaN composition and the roughly faceted surface morphology were not promising for subsequent growth of InGaN/GaN quantum-well active regions. As a result, our efforts turned towards exploration of 2-D nanopatterning of GaN and InGaN regrowth experiments on these 2-D patterns (see next discussion).

*Patterning and growth on nanoposts*

We subsequently began initial processing work on interferometric lithography of 2-D nanopatterns. The approach uses two superimposed interferometric-lithography (IL) exposures rotated by 60 degrees. Processing was optimized to transfer the pattern to photoresist, and a reactive-ion etching (RIE) procedure, with a chemistry tuned to PR and anti-reflective coating (ARC), was developed for transferring the 2-D nanopatterns into SiO2. The nanopatterns were transferred into the underlying GaN using the ICP-etching process followed by wet etching to remove sidewall tapering, using the procedures developed for the nanostripe work. This produced the *GaN nanopost arrays* upon which we grew InGaN.

We did our first InGaN regrowth on these GaN nanopost arrays using a 150-nm baseline thickness and intended composition of x~0.10 (although the actual composition in the planar spectator area turned-out to be only x~0.04). There was no In-incorporation on the sides or in a hexagonal crystalline cap structure that grew on top of the post. Analysis showed that In incorporated into an irregularly shaped deposit on the top / middle part of the posts.

We subsequently developed deposition and etching processes needed to *coat GaN nanopost arrays with a very thin layer of $SiO_2$*, with the intent to isolate subsequent GaN or InGaN regrowth to the tops of the posts by selectively masking growth elsewhere. The tops of the posts were cleared of $SiO_2$ by reactive-ion etching to provide a preferred site for the GaN regrowth. Because of concerns about possible plasma damage to the post-tops, and the possible removal of $SiO_2$ on the lower basal plane as well, we pursued a second, alternative design for making GaN posts with $SiO_2$-masked sidewalls (see next discussion). The first attempts at GaN regrowth on the post tops were unsuccessful, with unwanted growth on the post sidewalls in one case and in areas where the nanopattern was missing due to defects in patterning.

*Patterning and growth in nanohole arrays*

For this approach we developed metal-lift-off and etching processes needed to invert our nanopost patterns to *form nanohole arrays* in $SiO_2$ mask layers on GaN. Subsequent regrowth of GaN into these hole patterns were thought to provide an alternative path to the desired nanopost structures. The nanohole arrays in $SiO_2$ on GaN could also allow attempts to selectively grow InGaN directly on the nano-masked GaN as an alterative method for growing strain-relaxed InGaN.

To invert the post pattern and produce a mask with holes in it, we deposited a ~100-nm-thick Ni-metal layer on the surface of the PR nanopost array. This was followed by lift-off

of both the metal on top of the PR posts and the PR posts, then multiple RIE and wet-etching steps were used to fabricate nanohole arrays in the underlying 500-nm-thick $SiO_2$ layer on GaN/sapphire.

The first attempts at growing GaN in the nanoholes resulted in hexagonal pyramid structures in some of the holes and very small, incomplete crystallites in others. Growth for longer times produced more uniform arrays of the hexagonal pyramids, but the desired lateral growth over the $SiO_2$ was not observed.

In an attempt to further optimize the process, we grew a dilute InGaN underlayer and a three-period InGaN/GaN multi-quantum well on one of our GaN nano-pyramid arrays. The regrowth led to both nonselective InGaN/GaN growth on the $SiO_2$ mask and epitaxial InGaN/GaN growth on the exposed pyramidal facets of GaN.

The InGaN/GaN quantum-wells regrown on GaN nano-pyramids were characterized by room-temperature photoluminescence (PL) and panchromatic, spatially resolved cathodoluminescence (CL). The resulting InGaN/GaN heterostructures on the nano-pyramids showed emission at a broad range of wavelengths centered near 570 nm.

We worked to understand the origin of this long-wavelength emission. During this analysis, temperature-dependent PL measurements were initially mis-interpreted, leading us to incorrectly estimate an IQE for the sample in the range of 17-18%. The weak temperature-dependence observed in the PL intensities that gave rise to this overestimate of IQE was ultimately concluded to arise either because the observed yellow emission is defect related, or because competing non-radiative defect states do not completely freeze out and are able to modify the band-edge emission down to 4K, in which case the temperature dependence of the PL does not reveal the true IQE.

## Task 3: Growth of High-Indium-Composition Active Regions on Strain-Relaxed InGaN

*Regrowth of InGaN/GaN MQWs on {11-22} facets of pyramidal nanostripes*

After the processing difficulties were resolved, GaN was regrown on 350 nm nanostripes at 950 ºC. At short growth times, the stripe tops were flat with beveled edges indicating the onset of {11-22} facets. With further GaN regrowth, these facets evolve to a triangular or pyramidal sidewall profile forming the upper region of each stripe.

Growth of GaN was followed by a 5-period InGaN/GaN MQW, which produced the expected pyramidal stripe shape and {11-22} facets. Unlike our similar MQWs grown on pyramidal {10-11} GaN nanoposts using a $SiO_2$ mask, there was no obvious parasitic InGaN growth on the present $SiN_x$ mask, indicating significantly improved mask selectivity for $SiN_x$ versus $SiO_2$. In addition, we observed rows of pits, most likely v-defects, decorating the apices of some of the pyramidal stripes. Also, the {11-22} sidewall facets became corrugated, presumably because of the low-temperature-grown InGaN QW layers, which ultimately favor {10-11} and not {11-22} facet development. (A similar, but more-

striated, morphology was seen when we regrew thicker InGaN alloys on upright GaN nanostripe arrays in earlier experiments).

To determine the nominal quantum efficiency of the MQWs grown on {11-22} facets, MQWs concurrently grown on a planar (0001) GaN monitor template were also examined; both samples were benchmarked against previously grown, better-optimized (0001) green-emitting MQWs used in separately developed green LEDs. The facet-grown QWs emitted at ~516 nm, while the monitor-sample and benchmark-sample QWs emit at 523-532 nm. The small blue-shift probably results from loss of the Stark shift on moving the QWs from the polar (0001) plane to the semipolar {11-22} planes for the faceted regrowth.

Unfortunately, the {11-22}-facet-grown QWs had a peak intensity ~ 4X weaker than the (0001)-grown monitor QWs and ~ 16X weaker than our well optimized (0001) benchmark QWs, which are grown using an InGaN underlayer. We might expect that the facet-grown QWs and the monitor QWs would be ~4X brighter if they too were grown with InGaN underlayers. Even so, this would still leave the facet-grown QW active regions with subpar (~4X too low) internal quantum efficiency.

**Task 4: Optimization of InGaN p-doping**

Using p-doped InGaN layers, x~0.07-0.08, grown during Budget Period 2, additional optimization work was performed to investigate thermal activation annealing conditions for Mg dopants. Previous anneals performed in the growth reactor for 5 minutes under $N_2$ flow at 800 C were compared to newly performed anneals done *ex situ* in a RTE furnace for varying lengths of time and at different temperatures. The optimal RTE conditions were found to be 800 $^{o}$C for 5 minutes, very close to our standard *in situ* thermal anneal approach.

**Task 5: Evaluation of the internal quantum efficiency of deep-green emitters**

*Growth of nanopatterned LEDs*

Two MOCVD growth runs were performed to make prototype LED heterostructures. These structures incorporated GaN pyramidal nanostripes and facet-grown InGaN quantum wells. The main goal was to determine whether we could form a functional p-side structure on top of these nanopatterned quantum wells (QWs) in order to obtain electrical carrier injection into the patterned active-region. Given the early and unoptimized stage of the patterned QWs, it was not expected that these developmental test structures would deliver efficient electroluminescence.

For the first attempt, the LED was fabricated using a patterned MQW structure formed by an additional regrowth of a p-side heterostructure comprised of a ~200-nm-thick Mg-doped $Al_{0.15}Ga_{0.85}N$ electron-block layer followed by a ~250-nm-thick Mg-doped dilute InGaN layer. We found that the p-side regrowth ultimately covered the remaining openings to the $SiN_x$ mask. Continued low-temperature growth of the p-side InGaN partially preserved the initial pyramidal stripe shape, but the stripe widths became nonuniform and the pyramid height varied as the stripes evolved towards crystallographic facets other than the {11-22} facets seen at the end of MQW growth.

For testing comparisons, a second, structurally similar LED growth was performed, but with the important difference that it omitted the AlGaN electron-block layer. Additionally, the second LED was grown all in a single regrowth run on the as-fabricated nanopattern to avoid the multiple growth interrupts used for the first LED (the purpose of the interrupts was to allow SEM imaging studies of surface faceting and roughness as a function of growth thickness).

Electroluminescence spectroscopy of nanopatterned LEDs

To evaluate the electroluminescent properties of the LED structures, we employed a standard "quick test" procedure whereby indium metal dot contacts were applied to the top p-GaN surface of the LED and also in a scribe region that contacts the n-GaN layer. The indium contacts were distributed across the quarter-wafer pieces to evaluate spatial uniformity of electrical and optical performance. Samples were tested at 100 mA and light output was collected through the sapphire substrate using an optical fiber. Current-voltage characterization of the first regrown LED structure showed low voltage and no light emission in ~33% of the contacted regions, suggesting shorting of the LED junction in those regions. In contrast, the second LED structure, which was grown in a single growth run, showed a fairly uniform voltage performance and no shorting in any contact regions.

Both LED wafers showed lateral spatial variation of the electroluminescence intensity, most likely due to variations in the growth and patterning across the quarter-wafer surface. Of the electrically viable contact regions on sample 1, 75% of the regions showed a similar peak EL intensity, while 25% had low output. For sample 2, 33% of the contact regions showed relatively high light output, with 66% of the regions of notably lower light output.

We examined the electroluminescence (EL) spectra for the two patterned LED samples, as well as data from a reference LED wafer that was grown in the sample 2 growth run but on a planar 2"-diameter GaN-on-sapphire template. All of the samples, including the LED on planar GaN-on-sapphire, show broad spectral distributions. In the case of the planar reference sample, this breadth may have resulted from a roughened surface morphology caused by use of thicker than normal QWs depositions (~4.6 nm), which were needed to produce normal-thickness (~3 nm) QWs on the inclined {11-22} facets of the companion nanopatterned GaN template of actual interest.

The LEDs on the patterned templates exhibited unusual dominant wavelengths and reduced EL intensity compared to the planar reference. In particular, the sample 2 LED on a patterned template showed dominant red/near-IR emission that may be indicative of sub-bandgap defect emission. In separate EL experiments, a Si photodiode was employed to obtain a relative comparison of the integrated intensity of the sample 2 LED compared to our standard blue MQW LED quick test samples. Measurements at 20 mA revealed that the red/near-IR peaked emission from the sample 2 LED was on the order of 1000X weaker than the emission from a standard blue LED wafer, which again suggests defect-related emission. While the observed EL intensity is quite low, these first LEDs demonstrate that we could successfully achieve electrically injected luminescence from these nanopatterned devices.

## 3. Status of Project Milestones

The following Table summarizes progress towards the project milestones attained over the course of the project.

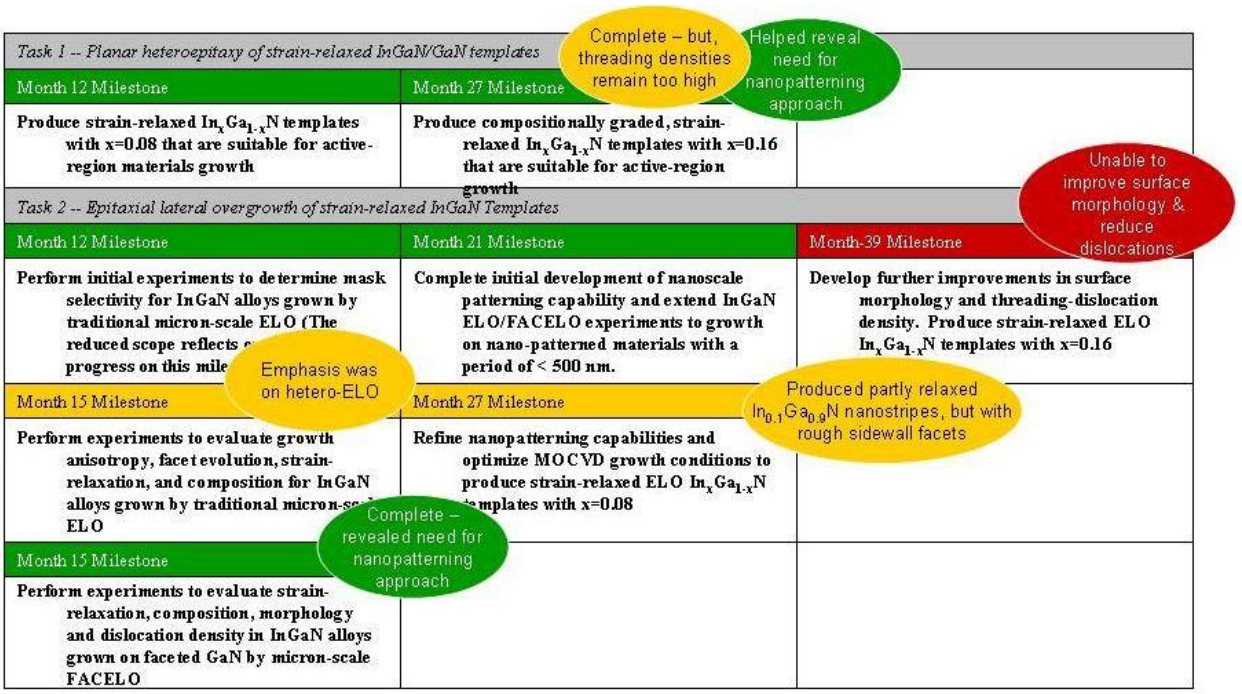


| *Task 1 -- Planar heteroepitaxy of strain-relaxed InGaN/GaN templates* | | |
|---|---|---|
| Month 12 Milestone | Month 27 Milestone | |
| **Produce strain-relaxed $In_xGa_{1-x}N$ templates with x=0.08 that are suitable for active-region materials growth** | **Produce compositionally graded, strain-relaxed $In_xGa_{1-x}N$ templates with x=0.16 that are suitable for active-region growth** | |
| *Task 2 -- Epitaxial lateral overgrowth of strain-relaxed InGaN Templates* | | |
| Month 12 Milestone | Month 21 Milestone | Month-39 Milestone |
| **Perform initial experiments to determine mask selectivity for InGaN alloys grown by traditional micron-scale ELO (The reduced scope reflects c… progress on this mile…** | **Complete initial development of nanoscale patterning capability and extend InGaN ELO/FACELO experiments to growth on nano-patterned materials with a period of < 500 nm.** | **Develop further improvements in surface morphology and threading-dislocation density. Produce strain-relaxed ELO $In_xGa_{1-x}N$ templates with x=0.16** |
| Month 15 Milestone | Month 27 Milestone | |
| **Perform experiments to evaluate growth anisotropy, facet evolution, strain-relaxation, and composition for InGaN alloys grown by traditional micron-sc… ELO** | **Refine nanopatterning capabilities and optimize MOCVD growth conditions to produce strain-relaxed ELO $In_xGa_{1-x}N$ …mplates with x=0.08** | |
| Month 15 Milestone | | |
| **Perform experiments to evaluate strain-relaxation, composition, morphology and dislocation density in InGaN alloys grown on faceted GaN by micron-scale FACELO** | | |

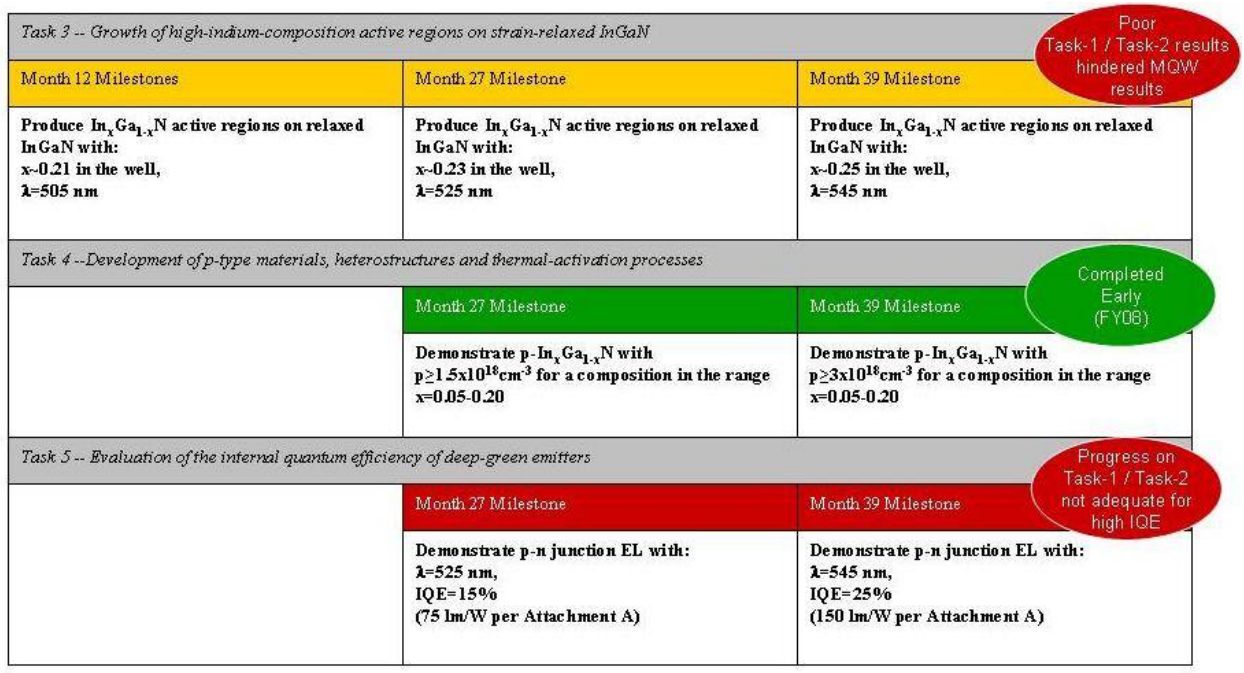


| *Task 3 -- Growth of high-indium-composition active regions on strain-relaxed InGaN* | | |
|---|---|---|
| Month 12 Milestones | Month 27 Milestone | Month 39 Milestone |
| **Produce $In_xGa_{1-x}N$ active regions on relaxed InGaN with: x~0.21 in the well, λ=505 nm** | **Produce $In_xGa_{1-x}N$ active regions on relaxed InGaN with: x~0.23 in the well, λ=525 nm** | **Produce $In_xGa_{1-x}N$ active regions on relaxed InGaN with: x~0.25 in the well, λ=545 nm** |
| *Task 4 --Development of p-type materials, heterostructures and thermal-activation processes* | | |
| | Month 27 Milestone | Month 39 Milestone |
| | **Demonstrate p-$In_xGa_{1-x}N$ with $p \geq 1.5 \times 10^{18} cm^{-3}$ for a composition in the range x=0.05-0.20** | **Demonstrate p-$In_xGa_{1-x}N$ with $p \geq 3 \times 10^{18} cm^{-3}$ for a composition in the range x=0.05-0.20** |
| *Task 5 -- Evaluation of the internal quantum efficiency of deep-green emitters* | | |
| | Month 27 Milestone | Month 39 Milestone |
| | **Demonstrate p-n junction EL with: λ=525 nm, IQE=15% (75 lm/W per Attachment A)** | **Demonstrate p-n junction EL with: λ=545 nm, IQE=25% (150 lm/W per Attachment A)** |

## 4. Products Developed & Technology Transfer Activities

None.

The main result of this project is unpublished research data. These data are described in further detail in the 36 monthly reports, two annual reports, one peer-review evaluation report, and multiple technical presentations submitted to DOE/NETL over the course of the project. The present final report consists of selected excerpts from these previous reporting efforts.